

BRIEF COMMUNICATION OPEN

Photocatalytic activity of twist-angle stacked 2D TaS₂Evgeniya Kovalska¹✉, Pradip Kumar Roy¹, Nikolas Antonatos¹, Vlastimil Mazanek¹, Martin Vesely², Bing Wu¹ and Zdenek Sofer¹✉

The low-cost, efficient photoelectrosensitive electrodes as an alternative to expensive and complex rigid systems are yet in demand for advanced photoresponsive technology. Here, the light-induced efficiency of electrochemically exfoliated TaS₂ nanosheets for hydrogen generation catalysis and photodetectors was demonstrated. Mutual twisting of the exfoliated 2H-TaS₂ flakes leads to the redistribution of charge density induced by interlayer interaction of the individual nanosheets. External light irradiation on the TaS₂ surface influences its conductivity making the material feasible for photoelectrocatalysis and photodetection. The TaS₂-based photoelectrocatalyst demonstrates high hydrogen evolution reaction (HER) activity with the onset overpotential below 575 mV vs. reversible hydrogen electrode (RHE). The TaS₂-integrated photodetector in the acidic medium represents its broadband response with the highest photoresponsivity (0.62 mA W⁻¹) toward 420 nm light illumination. This finding will pave the way to a new realization of exfoliated twist-angle stacked TaS₂ for photo-induced electrochemistry and sensing.

npj 2D Materials and Applications (2021)5:68; <https://doi.org/10.1038/s41699-021-00247-8>

INTRODUCTION

With increasing demands in modern society, the energy crisis and environmental problems are currently in the spotlight. Hydrogen is the main sustainable source of renewable energy and is highly required for advanced energy conversion systems. Recently, photoelectrocatalytic and photoelectrochemical water-splitting methods are an efficient approach for the scalable generation of hydrogen. The concept of light-induced energy production through semiconductor catalysts attracted many research efforts aiming at the development of low-cost, efficient bifunctional materials for hydrogen production and environment-sensing response. The performance of these materials can be tuned while illuminating the light of various wavelengths. The occurred photo-induced electron transfer in the targeted nanosheets-based sensitive material will generate photoelectrochemical water splitting, e.g., faster hydrogen evolution reaction (HER) or broadband light-sensitive detector. These will pave new ways for emerging materials as a cheaper and more productive alternative to most common fossil fuels-based methods of hydrogen production as well as traditional photodetectors.

Two-dimensional (2D) transition-metal dichalcogenides (TMDs) have been demonstrated as promising catalysts for water splitting, hydrogen reduction, and water oxidation^{1,2}. The unique chemical and physical properties of 2D TMDs are demonstrated by their small size enriched by the number of edge active sites, band-edge position, quantum confinement effect and thus, exhibit photo-induced catalytic efficiency³. TMDs are considered the most promising cost-effective catalysts, and their properties are determined by the TMDs' polymorph type, namely hexagonal 2H or trigonal 1T. It has been reported that stable 2H-MoS₂ shows semiconducting properties; meanwhile, metastable 1T-MoS₂⁴ or 1T-WSe₂⁵ forms demonstrate metallic properties. The metallic phase of a material is capable of a more efficient performance than the semiconducting 2H counterpart due to its enhanced electrical conductivity. The metallic character is associated with undercoordinated chalcogen atoms at the 1010 edge of 2D TMD, providing more efficient adsorption of hydrogen, which is a crucial step for electrochemical water splitting⁶. The MoS₂ and WSe₂

exhibit superior catalytic activity and are used as alternatives to Pt-based catalysts⁷⁻⁹. The WSe₂ is demonstrated as an excellent output stability photodetector due to its high absorption coefficient in the visible and near-infrared regions^{10,11}. Other known 2D materials, such as TiSe₂¹²⁻¹⁴, NiSe₂^{15,16}, TaSe₂¹⁷, and TaS₂¹⁸⁻²⁰, are interesting due to their superconductivity, charge-density wave, and metal-insulator transitions.

Among other 2D TMD materials, tantalum disulfide (TaS₂) has been subject to numerous studies due to the variety of the material's unique structural and electronic phases²¹. Its initial metallicity and, thus, electrical conductivity can lead to potential applications such as a light-responsive active electrode in the HER and photosensing. Albeit the study of TaS₂ is mainly focused on the superconductivity²²⁻²⁴, field emission^{25,26}, photo-induced features of the material for HER and photosensing have not been explored yet. Aiming to enhance the photoresponse performance of the TaS₂, the quality and dimensions of the material must be considered. For instance, bulk TaS₂ lacks exposed active sites that significantly affect the conversion efficiency of the material and narrows its application. Therefore, a thorough cleavage of the van der Waals structure by selecting the most appropriate method is essential to increase the conversion efficiency of TaS₂.

Several methods have been demonstrated to produce layered TaS₂, such as chemical vapor deposition (CVD)²⁷, mechanical cleavages²¹, intercalation²⁸, ultrasonication²⁹⁻³¹, or liquid-phase exfoliation²². However, the CVD method remains to be improved before it can be used to produce large-domain homogeneous TaS₂ films. The mechanical cleavage is not scalable and undergoes a lack of control over product thickness and size. Alternatively, electrochemical exfoliation (one of the solution-based techniques) is the most convenient, controlled, and straightforward method that can be employed in ambient temperature for large-scale production of 2D TaS₂. Recently the electrochemical approach has been successfully applied to exfoliate few-layer phosphorene³² and arsenene³³ and has been pioneered for single-step production of platinoid-decorated phosphorene³⁴.

Therefore, in this study, the photoresponse of electrochemically exfoliated TaS₂ nanosheets which have preliminarily been

¹Department of Inorganic Chemistry, University of Chemistry and Technology Prague, Technická 5, Prague 166 28, Czech Republic. ²Department of Organic Technology, University of Chemistry and Technology Prague, Technická 5, Prague 166 28, Czech Republic. ✉email: evgeniya.kovalska.ua@gmail.com; soferz@vscht.cz

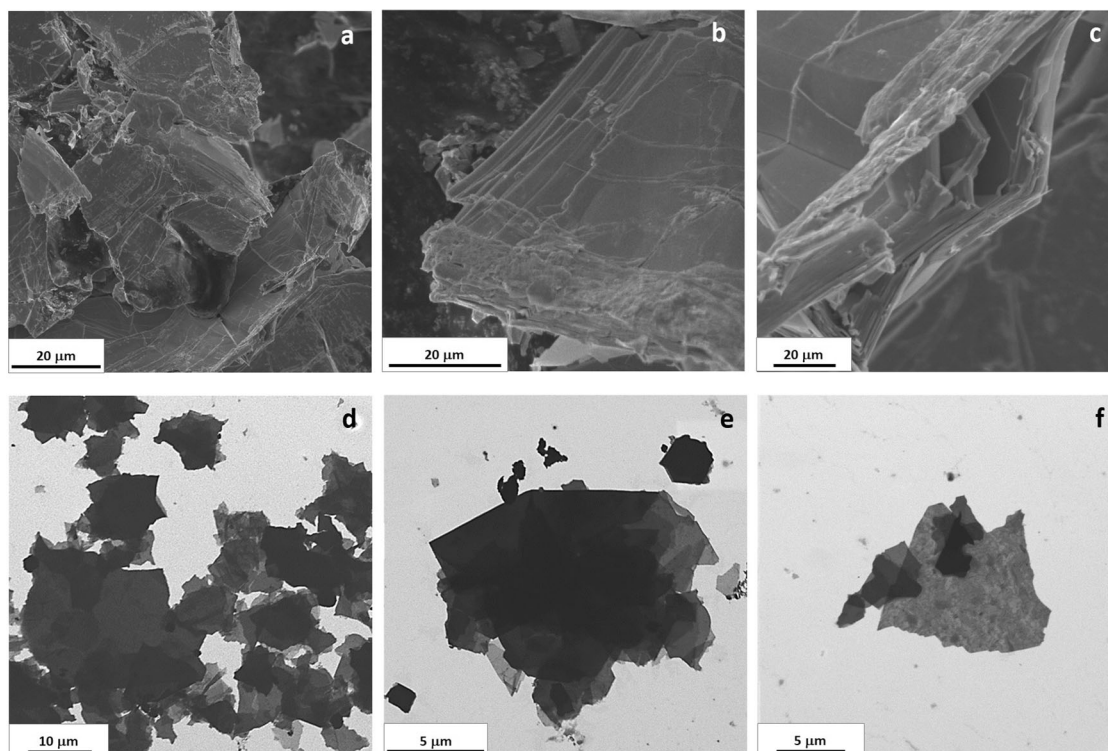


Fig. 1 Morphological characterization. SEM images (a–c) of bulk TaS₂ and STEM images (d–f) of exfoliated 2D TaS₂ nanostructures.

characterized by micro- and spectroscopic techniques (Supplementary Notes 1) was investigated in an effort to develop a low-cost, efficient photosensitive electrode that can replace noble metal-based catalysts³⁵ (as a photoelectrocatalyst—PEC) and CMOS-based photodetectors³⁶ (as a photodetector—PD). Pioneered low-potential electrochemical exfoliation of TaS₂ crystals was carried out in a nonaqueous electrolyte medium of tetrabutylammonium hexafluorophosphate (TBAPF₆) in N, N-dimethylformamide (DMF). The as-exfoliated 2D TaS₂ nanostructures consist of few-layer nanosheets and nanoparticles. Detailed characterization of bulk and exfoliated TaS₂ was performed through various microscopic and spectroscopic techniques. The photo-induced high HER electrocatalytic activity of the as-exfoliated TaS₂ nanostructures with low overpotential (>575 mV and 320 mV) was reported. A room-temperature TaS₂-based broadband photodetector in the acidic medium of 0.5 M H₂SO₄ has been presented. The higher electrical conductivity of 2D TaS₂ compared to its bulk form can improve the efficiency of charge distribution in the catalytic/sensing systems and, thus, broaden the material's application area.

RESULTS

Synthesis and characterization of the materials

Electrochemical exfoliation of bulk TaS₂ crystal [see scanning electron microscopy (SEM) images in Fig. 1a–c] was performed in anhydrous electrolyte of 0.01 M TBAPF₆ in DMF. Following three main steps of the procedure, namely wetting of the crystal, accumulation (or activation) of the tetrabutylammonium cations (TBA⁺), and their intercalation between TaS₂ layers were carried out at –1, –2.5, and –3.8 V (vs. 0.1 M Ag/AgNO₃), respectively. The first two steps were completed in 2 min each, followed by 4 h of TBA⁺-assisted intercalation-delamination process at a potential of –3.8 V. It has to be noted that the duration of the process is defined by the initial size of the TaS₂ crystal and can be

terminated when a sufficient amount of the exfoliated material is produced.

After the exfoliation of the TaS₂ crystal, flakes of various sizes and thicknesses were observed in the resulted dispersion based on STEM (Fig. 1d–f) and AFM analysis (Fig. 2). These include TaS₂ nanosheets of lateral size up to 6 μm with a thickness of 30 nm and 2.3 μm nanosheets with 7 nm thickness. (Fig. 2a, b, respectively). In addition, exfoliated material consists of TaS₂ nanoparticles of 100–200 nm lateral size and thickness in the range between 0.5 and 3 nm. (Fig. 2c). The successful exfoliation of the TaS₂ crystal into nanosheets and nanoparticles, as well as their size distribution, were confirmed by the statistical analysis (Supplementary Fig. 1) obtained from STEM images. The results are also in good agreement with high-resolution TEM images (Supplementary Fig. 2) of two types of exfoliated nanostructures with a lateral size of ten-hundreds of nanometers and several micrometers.

TEM and SAED microscopies demonstrate good quality of exfoliated TaS₂ nanosheets (Fig. 3a–d) of hexagonal structure (schematic image, Fig. 3e, f). High-resolution TEM images in Supplementary Fig. 3 also show the formation of round-shaped TaS₂ nanoparticles localized on the surface of the larger flakes. This is consistent with the statistical analysis of particle size distribution (Supplementary Fig. 1) that confirms the production of two types of TaS₂ nanostructures. Based on the fast Fourier transform (FFT) analysis of TEM images (Supplementary Fig. 4), the crystal symmetry of TaS₂ is demonstrated as the fringes oriented in a three-fold rotation axis. The d-spacing of the symmetry of the TaS₂ crystal of about 2.9 Å and 2.93 Å defines its (100) planes' orientations. The electron diffraction patterns of a flat area of the TaS₂ nanosheet show this growing direction. Different magnification TEM images of the TaS₂ exhibit in-plane atoms are ordering with the lattice spacing of 0.305 nm. The morphology of the exfoliated material and thus sharply defined layered appearance are caused by the initial structure of the TaS₂ crystal.

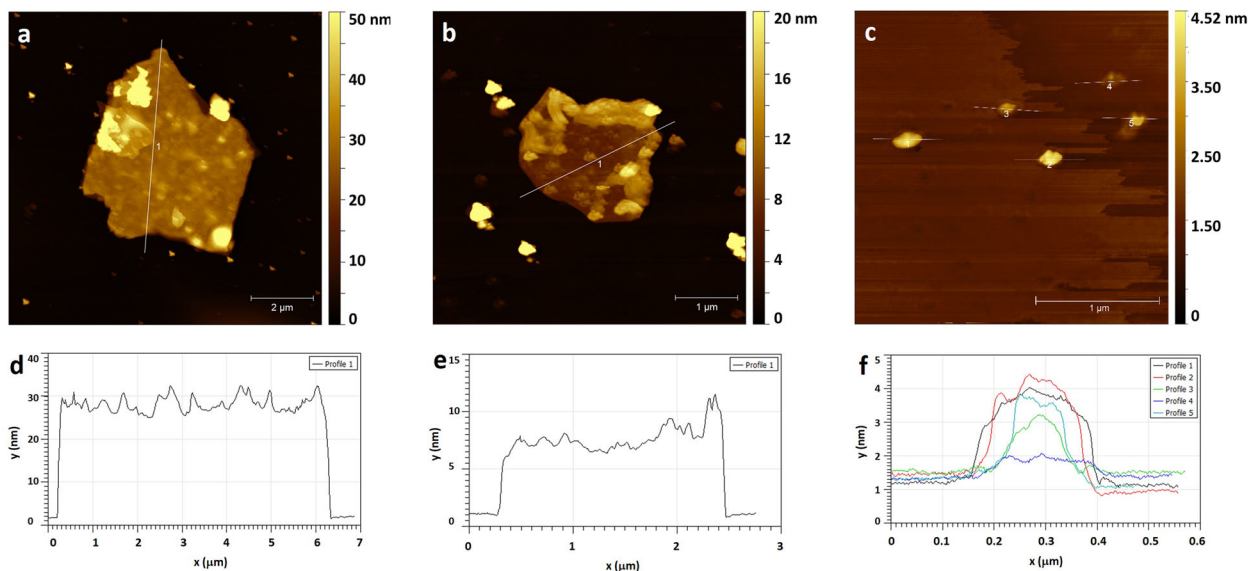


Fig. 2 Topographic imaging. AFM images of the as-exfoliated TaS₂ nanosheets (**a**, **b**), nanoparticles (**c**), and their corresponding height profiles (**d**–**f**).

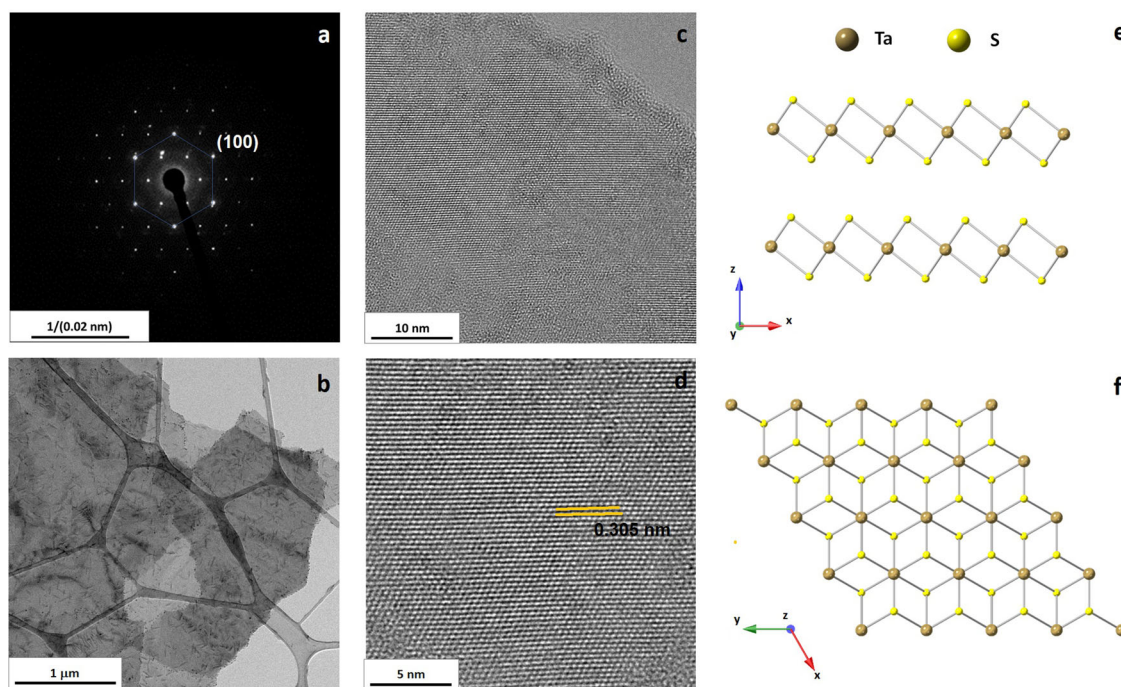


Fig. 3 SAED and TEM analysis of electrochemically exfoliated TaS₂. **a** SAED pattern; **b** low-resolution TEM image; **c**, **d** high-resolution TEM images; schematic **e** side and **f** top views of the TaS₂ structure.

The SAED patterns of the large area TaS₂ flakes (Supplementary Fig. 5) verified several configurations of 2H-type structure with the different twist angles of 7°, 8°, 9°, and 10° (Fig. 4). The value of twist angle of as-exfoliated TaS₂ nanosheets is relatively regular for all analyzed samples (7–10 degrees) and increases between rows: 1 layer < 2 layers < 3 layers. The trigonal arrangement of Ta atoms in Fig. 3e, f corresponds to the standard stacking of S-Ta-S in the unit cell. This direct stacking of each layer via Ta atoms was theoretically proven in a few publications^{37,38}; however, experimentally was confirmed only for 1T-TaS₂ bilayer structure³⁹. Based on the density of state calculations, the electronic properties of the 1T-TaS₂ bilayer depend on the twist angles. The increase of both formation energy and bandgap has been theoretically

explained due to the interlayer interaction of twisted TaS₂ flakes and the redistribution of charge density induced by the in-plane distortion³⁸. This feature can also lead to the increase of the electronic specific-heat coefficient of the randomly twisted TaS₂ nanosheets²², establishing the material as a promising candidate for photo-induced applications⁴⁰.

The analysis of the crystal structure and optical characteristics of the bulk and exfoliated TaS₂ is demonstrated in Fig. 5. X-ray diffraction (XRD) was used to verify the successful synthesis of hexagonal 2H-TaS₂ (Supplementary Notes 2, 3). The XRD pattern in Fig. 5a confirmed the *P-3m1* hexagonal structure of TaS₂ (PDF: 04-003-4190). No other phases were observed, indicating the purity of the starting material. The sharp peaks in the pattern

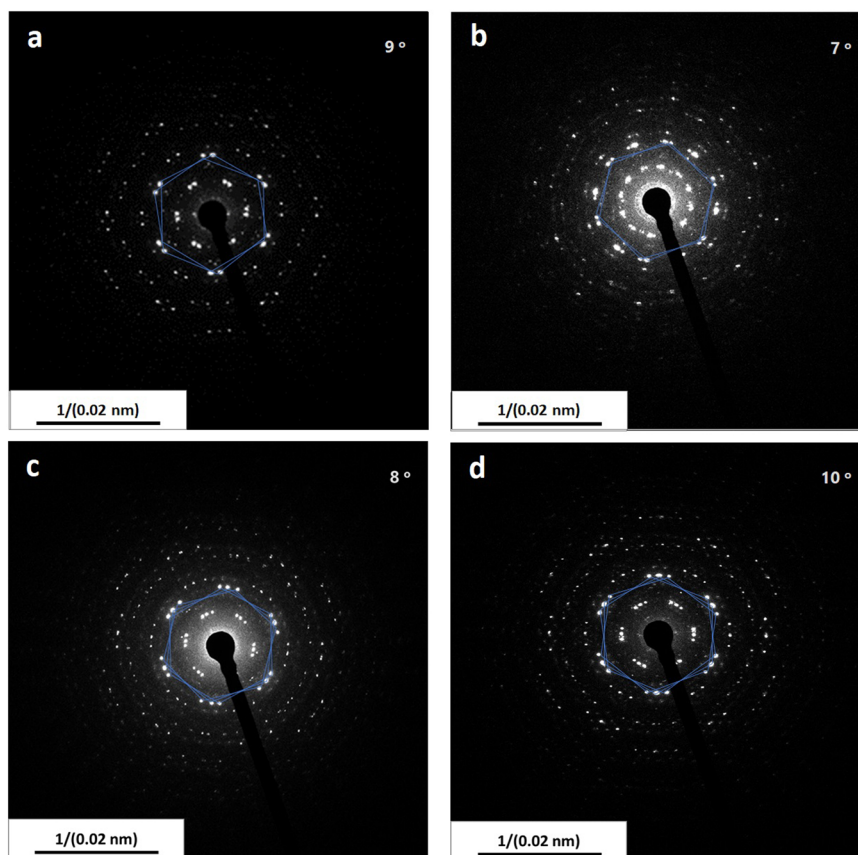


Fig. 4 The distribution of various twist angles of a few-layer TaS₂. The SAED patterns taken from a large area refer to the various twist of the **a, b** bilayer and **c, d** three-layer TaS₂.

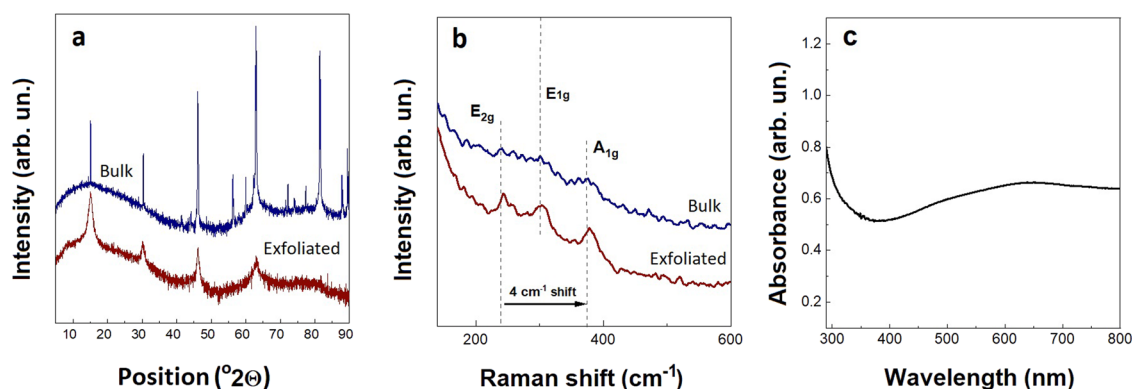


Fig. 5 Structural and optical characteristics of TaS₂. **a** XRD diffractogram of bulk TaS₂ and electrochemically exfoliated nanosheets; **b** Raman spectra of bulk and electrochemically exfoliated TaS₂; **c** UV-VIS absorbance spectra of the exfoliated TaS₂ in the DMF.

ascertaining the high crystallinity of the sample. Similar peaks were observed in the exfoliated material's XRD pattern, albeit broadened and with lower intensity caused by the disruption of initial crystallinity due to the exfoliation procedure. The broadening of the XRD peaks indicates a decrease in crystal size and lattice strain increase. Figure 5b shows the Raman spectra of bulk and as-exfoliated TaS₂ samples. Three main Raman features depicted at 239, 301, and 373 cm⁻¹ from the bulk crystal were assigned to the E_{2g}, E_{1g}, and A_{1g} modes, respectively^{28,41}. More prominent peaks of the same modes and their 4 cm⁻¹ redshifts were observed for the exfoliated nanosheets. The shift is attributed to the decrease of the interlayer van der Waals forces and the material's thickness reduction. UV-VIS absorption spectrum of the as-exfoliated TaS₂ nanostructures recorded at room

temperature is demonstrated in Fig. 5c. The TaS₂ represents low in-plain reflectivity at high energies (from 400–720 nm) and vice versa at low energies accordingly⁴².

To confirm chemical composition and binding states, we have measured the survey (Supplementary Fig. 6) and high-resolution X-ray photoelectron spectra (HR-XPS) of Ta 4f and S 2p (Fig. 6). Survey spectra confirmed composition, which was close to TaS₂ for bulk and exfoliated samples as well. Since exfoliated samples were measured on a gold substrate, Au peaks can also be seen in its survey spectrum. HR-XPS Ta 4f spectra were deconvoluted with two binding states Ta^{IV} (TaS₂) and Ta^V (Ta₂O₅), with binding energies 22.9 and 26.1 eV, respectively⁴³. Although O 2s at 24.0 eV overlaps with the Ta 4f, it was not used for deconvolution because its amount was less than 1% due to a low relative sensitivity factor

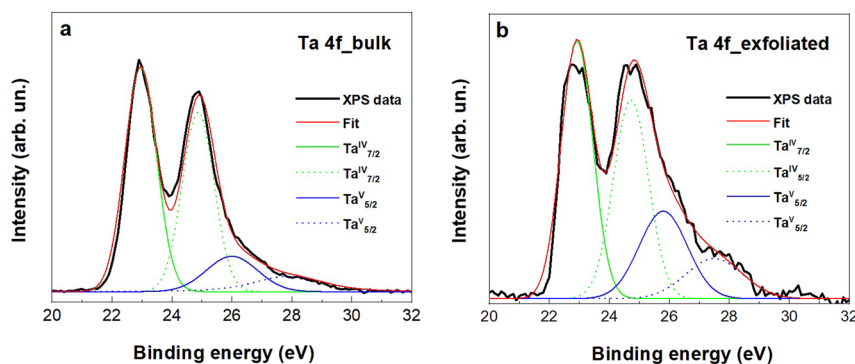


Fig. 6 Chemical composition and binding states of TaS₂. High-resolution XPS spectra of the **a** bulk and **b** electrochemically exfoliated TaS₂ nanostructures.

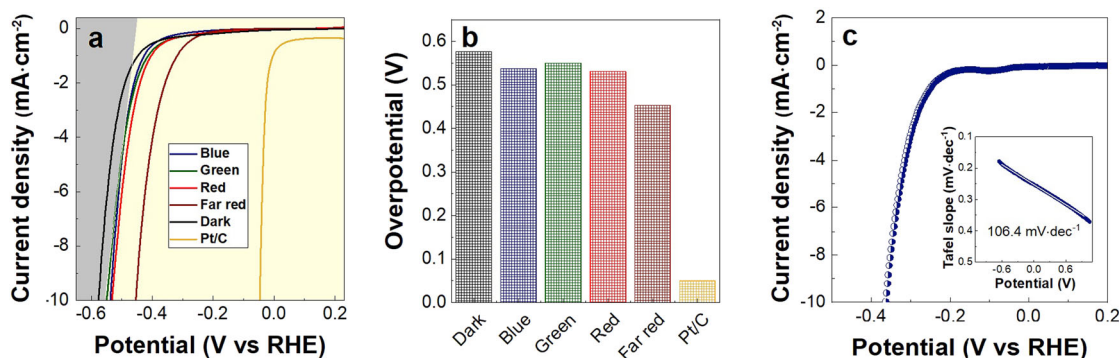


Fig. 7 Catalytic performance of a few-layer TaS₂ in HER. HER analysis in the medium of 0.5 M H₂SO₄ at the scan rate of 1 mV·s⁻¹ in dark mode and during the blue, green, red, and far-red illumination. Polarization curves **(a)** and corresponding overpotentials **(b)** of exfoliated TaS₂ at a -10 mA cm^{-2} current density; the measurements were conducted vs. RHE and compared with commercial Pt/C electrocatalyst. The gray and purple areas on the graph **(a)** correspond to the position of the polarization curves during the measurement in dark and illumination modes. Polarization curve and inserted corresponding Tafel plot **(c)** of few-layer TaS₂ small flakes obtained after centrifugation; overpotential is 360 mV.

of 0.14 compared to 8.62 for Ta 4f. Each binding state in Ta 4f has spin-orbit components separated by 1.92 eV. Binding state ratios are summarized in Supplementary Table 1. Bulk crystal was covered by 20% of Ta₂O₅, and after exfoliation, this amount increased to 30%. It has to be noted that TaS₂ is susceptible to oxidation, and this ability is even higher after the exfoliation⁴³. Thus, operating the material in an oxygen-free environment and storing it in the dry solvents will increase the stability of as-exfoliated TaS₂.

Photoelectrocatalytic performance of as-exfoliated TaS₂ for HER

Light-driven electrocatalysis using semiconducting materials (e.g., TaS₂) or their heterostructures is one of the most promising sustainable approaches for hydrogen generation by water splitting^{44–46}. Even though a thermal treatment or catalyst support texturization of the catalytic films is used to increase the number of active centers of the TaS₂ flakes, these methods are time-consuming and require a high-temperature and inert gas atmosphere⁴⁷. The light-induced electrochemistry (photoelectrochemistry) can be a simple approach to enhance the HER activity of the TaS₂ nanosheets. To the best of our knowledge, the photoelectrocatalytic activity of TaS₂ has not been explored to date.

Herein, the photoelectrocatalytic performance of electrochemically exfoliated TaS₂ for HER was explored (see Supplementary Notes 4). The three-electrode linear sweep voltammetry (LSV) was performed in the 0.5 M H₂SO₄ employing a few-layer TaS₂ deposited on a glassy carbon as a working electrode. The measurements have been repeated in the light mode for four

different wavelengths (420, 532, 630, and 720 nm). In addition, the results were compared with the dark mode for as-exfoliated TaS₂ nanosheets of mixed composition. The mixed composition consists of nanosheets of various sizes and nanoparticles, as was confirmed by the AFM, STEM, and statistical analysis. Few-layer TaS₂ samples of a smaller lateral size ($\sim 30\text{--}40 \text{ nm}$, Supplementary Fig. 7) were obtained as follows: first, the TaS₂ dispersion was centrifuged at 3500 rpm for 10 min; second, the collected supernatant was centrifuged at 10,000 rpm for 10 min, and the resulting precipitate was used for the test.

As shown in Fig. 7a, b, the HER for initial as-exfoliated TaS₂ starts at a potential of 575 mV (vs. RHE) under dark mode at a current density of 10 mA cm^{-2} . Under the illumination light of different wavelengths, the overpotential shifts towards lower potentials, specifically: 537, 549, 531, and 454 mV when blue, green, red, and far-red light-emitting diodes (LEDs) are implemented, respectively. This behavior is attributed to the carrier increment generated in the TaS₂ nanosheets with light irradiation enhanced by the intrinsic defect (wrinkles) and mutual twisting of the individual layers. The current density of the TaS₂ catalyst under dark decreases after 100 cycles (Supplementary Fig. 8), demonstrating a slow degradation of the as-investigated catalyst. It has to be noted that the onset overpotential for the TaS₂ catalyst based on flakes of smaller size was significantly reduced to $\sim 320 \text{ mV}$ (Fig. 7c). Considering the influence of the light on the as-exfoliated samples, the $\sim 100 \text{ mV}$ decrement of the overpotential is expected that will make a few-layer TaS₂ a superior HER photoelectrocatalyst. This study on bare TaS₂ catalysts can compete with recently reported results⁴⁸, where the performance of TaS₂ was enhanced by the incorporation of conductive films⁴⁹ or thermal treatment in the H₂-environment⁴⁷.

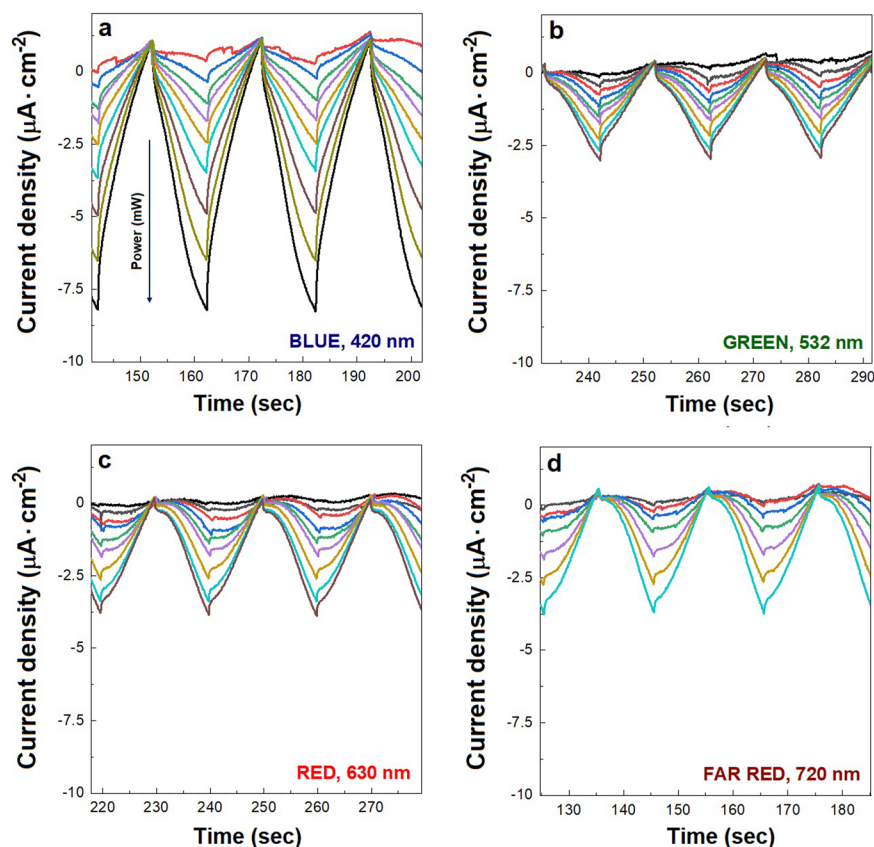


Fig. 8 TaS₂-integrated photodetector. Power dependence of photocurrent density under the illumination of **a** blue (420 nm), **b** green (532 nm), **c** red (630 nm), and **d** far-red (720 nm) LED sources in 0.5 M H₂SO₄ solution at 0.5 V vs. SCE. The power increased from 100 to 1200 mW: an arrow in **a** demonstrates the direction of LED power increment, which applies to all lights (**b–d**).

Furthermore, thoroughly prepared catalysts under light illumination will outperform the HER activity of commercial Pt/C electrode (~40 mV), providing a cheaper alternative.

TaS₂-integrated photodetector

Solution-based PDs offer unique advantages over standard photodetectors in the form of a simple and easy device manufacturing process. Recently 2D nanomaterials have demonstrated their feasibility for PDs ranging from visible to THz; however, this is not inherent to one material^{42,50,51}. Therefore, a broadband photodetection capability of materials is highly demanded to its wide application possibility. The intrinsic parameters of the material's light sensitivity and response can be tuned by changing the applied voltage, analyte concentration, and power of the illuminated light. Herein, the photoelectrochemical response of TaS₂ in a 0.5 M H₂SO₄ acidic medium was measured in a three-electrode system at ambient temperature. The TaS₂-integrated PD was tested under four illumination wavelengths (420, 520, 630, and 720 nm) with a scanning speed of 10 mV·s⁻¹. The procedure of the electrode preparation and photoelectrochemical measurements are described in Supplementary Notes 5.

The results illustrating a steady response toward different illumination wavelengths are depicted in Fig. 8. As shown in Fig. 8a, the power-dependent photocurrent measurement was achieved by using chronoamperometry in 0.5 M H₂SO₄ at 0.5 V against saturated calomel electrode (SCE) under the illumination of a 420 nm blue LED light source. The response of the TaS₂-based electrode toward blue illumination was the highest in comparison with other LEDs. The response toward green illumination (Fig. 8b) was decreased and slightly increased after applying red (Fig. 8c)

and far-red (Fig. 8d) light sources. The most prominent response of the electrochemically exfoliated few-layer TaS₂ is demonstrated under blue illumination and well consistent with the light absorbance of the material (Fig. 5d). The near-linear increment in current density with the increase of the illumination power from 100 to 1200 mW was illustrated (Supplementary Fig. 9a) for all lights. Additionally, I–V measurements were performed using LSV with a scanning speed of 20 mV·s⁻¹ and under continuous blue light illumination with the power of 600 mW (Supplementary Fig. 9b). The results display an increment in photocurrent with the increase of applied voltage, demonstrating the maximum photoelectrochemical performance of the TaS₂ nanosheets in 0.5 M H₂SO₄ at around –0.6 V vs. SCE. As the intensity increases, the current response jumps to a higher value corresponding to a higher conductance, indicating that the separation of electron-hole pairs is triggered.

The photodetection potential of the material has been assessed in more detail by calculating a few essential parameters. At first, the photoresponsivity (R_{ph}) of the TaS₂-integrated PD has been calculated using the following equation: $R_{ph} = \Delta I/P$, where ΔI represents the difference in photocurrent density between the dark and photocurrent, and P is the irradiation power intensity per unit area. The calculated photoresponse demonstrated the highest responsivity of about 0.62 mA·W⁻¹ under a 420 nm blue LED source illumination at 0.5 V applied potential (vs. SCE). Figure 9a highlighted the photoresponsivity of the devices concerning the power for different illumination wavelengths. Another important parameter for the evolution of photodetection capability is specific detectivity; it has been determined accordingly⁵²

$$D^* = \frac{(AB)^{1/2}}{NEP} \quad (1)$$

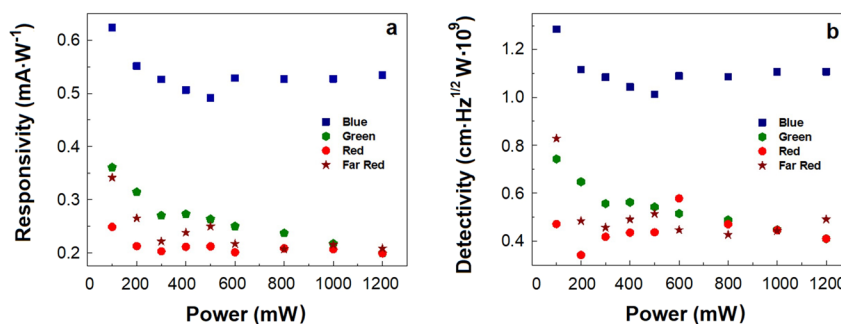


Fig. 9 Photoelectrochemical performance of TaS₂-integrated photodetector. The responsivity (a) and specific detectivity (b) of TaS₂-integrated PD in 0.5 M H₂SO₄ solution as a function of power upon four different illumination wavelengths: blue, green, red, and far-red.

In the above equation, A , B , and NEP stand for the active area, measured bandwidth, and noise equivalent power, respectively. NEP is defined as the input signal power resulting in a signal-to-noise ratio (S/R) of 1 in a 1 Hz output bandwidth. Furthermore, in the equation form, NEP can be presented as^{52,53}

$$NEP = \frac{I_N}{R_{ph}} \quad (2)$$

Here, R_{ph} and I_N represent the photoresponsivity of the PD and the noise current, respectively. In addition, the noise, which is associated with the dark current (I_D) of the PD current, can be ascribed as $I_N^2 = 2eI_D B$, where e represents the electronic charge⁴². The calculated specific detectivity of our PD devices of about $1.28 \times 10^9 \text{ cm}\cdot\text{Hz}^{1/2}\cdot\text{W}^{-1}$ (Fig. 9b).

Prepared TaS₂-based PD exhibited a broadband photodetection capability with the highest photoresponsivity ($0.62 \text{ mA}\cdot\text{W}^{-1}$) and specific detectivity ($1.28 \times 10^9 \text{ cm}\cdot\text{Hz}^{1/2}\cdot\text{W}^{-1}$) toward 420 nm light illumination, which is nearly double compared with 532, 630, and 720 nm illumination wavelengths. This photoresponsivity value is higher than the response of solution-based photodetectors integrated with other TMDs (Supplementary Table 2). Our results demonstrate the versatility of 2H-TaS₂-based PD, which exhibits metal-like characteristics coupled with broadband light absorption and thus emission due to energy-separated bands. The original metallicity of the TaS₂ that is assisted by undercoordinated atoms at edge sites is enhanced by the random twisting between the TaS₂ monolayers, which form a rich homogeneous interface with enhanced conductivity²². This consequently increases the electron transfer in the “TaS₂ electrode/0.5 M H₂SO₄ electrolyte” system and thus improves the catalytic performance of the material, establishing it favorable for electrocatalysis^{1,2,43}.

DISCUSSION

The light-induced efficiency of electrochemically exfoliated TaS₂ for photoelectrocatalysis and photodetector performance has been demonstrated. A well-controlled exfoliation process that is based on the TBA⁺-cation intercalation between the TaS₂ interlayers was performed in the nonaqueous DMF medium applying a potential of -3.8 V . Few-layer TaS₂ nanosheets of different lateral sizes, namely, 10–100 nm and 1–30 μm , were identified and characterized by numerous characterization and microscopy techniques. It was shown that exfoliated TaS₂ nanosheets possess a trigonal prismatic structure (2H type, hexagonal) and, thus, metallic character. The metallicity of the 2H-TaS₂ nanosheets was enhanced by the twisting of the individual flakes and their mutual interaction, causing charge-density redistribution. This ability was further increased by the external illumination of the light of the following wavelengths: 420 nm (blue), 532 nm (green), 630 nm (red), and 720 nm (far-red). Based on the above, TaS₂ nanosheets were tested as PEC for HER and PD of visible light. The as-exfoliated TaS₂-based catalyst,

under light illumination, demonstrated high HER catalytic activity with the overpotential for $-10 \text{ mA}\cdot\text{cm}^{-2}$ below 575 mV, which is $\sim 100 \text{ mV}$ lower than during dark mode. Additionally, it was proven that the accurate preparation of the TaS₂-based catalyst via sample centrifugation can significantly enhance the catalytic performance of the material. Solution-processed TaS₂-enabled PD exhibited broadband light sensitivity in the visible range. The highest photoresponsivity ($0.62 \text{ mA}\cdot\text{W}^{-1}$) and specific detectivity ($1.28 \times 10^9 \text{ cm}\cdot\text{Hz}^{1/2}\cdot\text{W}^{-1}$) were observed under blue light illumination, nearly double compared to green, red, and far-red lights. These findings can potentially ignite multiple insights of 2H-TaS₂ in photo-induced electrochemistry and (nano)optoelectronics.

METHODS

Synthesis and crystal growth

TaS₂ crystals were grown by the vapor transport method in quartz glass ampoule using iodine as a transport medium. For the synthesis were used tantalum (powder—200 mesh; 99.9%) and sulfur (99.9999%, granules) corresponding to 10 g of TaS₂ were placed together with 250 mg of iodine (granules, 99.9999%) in quartz glass ampoule (35 \times 180 mm) and melt sealed under high vacuum ($1 \times 10^{-3} \text{ Pa}$). The ampoule was first heated at 600 °C for 50 h, following 50 h of treatment at 800 °C and 1000 °C. The vapor transport was performed at 1000 °C for the hot zone with the TaS₂ charge and 950 °C for the cold crystal growth zone for seven days. Formed hexagonal crystals with sizes up to 20 mm were separated from the ampoule in the glovebox.

Electrochemical exfoliation

The electrochemical exfoliation of TaS₂ crystal was carried out in the organic-based electrolyte composed of 0.01 M TBAPF₆ in DMF. The procedure was conducted in the four-port electrochemical cell equipped with a reference (0.1 M Ag/AgNO₃ in acetonitrile), counter (platinum), and working (TaS₂ crystal) electrodes as well as argon purging. Three different potentials were applied to the working electrode to initiate its wetting at -1 V for 120 s, activate the tetrabutylammonium cations (TBA⁺) at -2.5 V for 120 s, and finally stimulate cations' intercalation between TaS₂ interlayers at -3.8 V for several hours. As-exfoliated TaS₂ precipitate was collected, ultrasonicated for 30 min, and then washed in several polar organic solvents (acetonitrile, methanol, and DMF) using vacuum filtration. The exfoliated TaS₂ was filtered through the cellulose membrane, redispersed, and stored in the dried DMF solution.

Electrocatalytic, photoelectrocatalytic measurements, and characterization

More details on the exploration of electrocatalytic and photoelectrocatalytic measurements and material characterization methods are given in the Supplementary Information file. B.W. was supported from the grant of Specific university research – grant No A2_FCHT_2021_055. P.K.R. was supported by the European Structural and Investment Funds, and CHEMFELLS III' (No.CZ.02.2.69/0.0/0.0/19_074/0014006).

DATA AVAILABILITY

The data that support the findings of this study are available from the corresponding author upon reasonable request.

Received: 3 March 2021; Accepted: 24 June 2021;

Published online: 22 July 2021

REFERENCES

- Voiry, D. et al. Conducting MoS₂ nanosheets as catalysts for hydrogen evolution reaction. *Nano Lett.* **13**, 6222–6227 (2013).
- Voiry, D. et al. Enhanced catalytic activity in strained chemically exfoliated WS₂ nanosheets for hydrogen evolution. *Nat. Mater.* **12**, 850–855 (2013).
- Li, Y., Li, Y.-L., Araujo, C. M., Luo, W. & Ahuja, R. Single-layer MoS₂ as an efficient photocatalyst. *Catal. Sci. Technol.* **3**, 2214–2220 (2013).
- Bai, S., Wang, L., Chen, X., Du, J. & Xiong, Y. Chemically exfoliated metallic MoS₂ nanosheets: a promising supporting co-catalyst for enhancing the photocatalytic performance of TiO₂ nanocrystals. *Nano Res.* **8**, 175–183 (2015).
- Liu, Q. et al. Stable metallic 1T-WS₂ nanoribbons intercalated with ammonia ions: the correlation between structure and electrical/optical properties. *Adv. Mater.* **27**, 4837–4844 (2015).
- Tsai, C., Chan, K., Nørskov, J. K. & Abild-Pedersen, F. Theoretical insights into the hydrogen evolution activity of layered transition metal dichalcogenides. *Surf. Sci.* **640**, 133–140 (2015).
- Johari, P. & Shenoy, V. B. Tuning the electronic properties of semiconducting transition metal dichalcogenides by applying mechanical strains. *ACS Nano* **6**, 5449–5456 (2012).
- Chhowalla, M. et al. The chemistry of two-dimensional layered transition metal dichalcogenide nanosheets. *Nat. Chem.* **5**, 263–275 (2013).
- Tan, C. & Zhang, H. Two-dimensional transition metal dichalcogenide nanosheet-based composites. *Chem. Soc. Rev.* **44**, 2713–2731 (2015).
- Chiriacescu, C. et al. Ultralow thermal conductivity in disordered, layered WS₂ crystals. *Science* **315**, 351–353 (2007).
- Li, H. et al. Mechanical exfoliation and characterization of single- and few-layer nanosheets of WSe₂, TaS₂, and TaSe₂. *Small* **9**, 1974–1981 (2013).
- Peng, J.-P. et al. Molecular beam epitaxy growth and scanning tunneling microscopy study of TiSe₂ ultrathin films. *Phys. Rev. B* **91**, 121113 (2015).
- Wang, J. et al. Controlled synthesis of two-dimensional 1T-TiSe₂ with charge density wave transition by chemical vapor transport. *J. Am. Chem. Soc.* **138**, 16216–16219 (2016).
- Joe, Y. I. et al. Emergence of charge density wave domain walls above the superconducting dome in 1T-TiSe₂. *Nat. Phys.* **10**, 421–425 (2014).
- Xi, X. et al. Strongly enhanced charge-density-wave order in monolayer NbSe₂. *Nat. Nanotechnol.* **10**, 765–769 (2015).
- Xi, X. et al. Ising pairing in superconducting NbSe₂ atomic layers. *Nat. Phys.* **12**, 139–143 (2016).
- Sun, S. et al. Direct observation of an optically induced charge density wave transition in TaSe₂. *Phys. Rev. B* **92**, 224303 (2015).
- Yu, Y. et al. Gate-tunable phase transitions in thin flakes of 1T-TaS₂. *Nat. Nanotechnol.* **10**, 270–276 (2015).
- Hovden, R. et al. Atomic lattice disorder in charge-density-wave phases of exfoliated dichalcogenides (1T-TaS₂). *PNAS* **113**, 11420–11424 (2016).
- Sipos, B. et al. From Mott state to superconductivity in 1T-TaS₂. *Nat. Mater.* **7**, 960–965 (2008).
- Tsen, A. W. et al. Structure and control of charge density waves in two-dimensional 1T-TaS₂. *PNAS* **112**, 15054 (2015).
- Pan, J. et al. Enhanced superconductivity in restacked TaS₂ nanosheets. *J. Am. Chem. Soc.* **139**, 4623–4626 (2017).
- Navarro-Moratalla, E. et al. Enhanced superconductivity in atomically thin TaS₂. *Nat. Commun.* **7**, 11043 (2016).
- Peng, J. et al. Disorder enhanced superconductivity toward TaS₂ monolayer. *ACS Nano* **12**, 9461–9466 (2018).
- Zong, P.-A. et al. Flexible foil of hybrid TaS₂/organic superlattice: fabrication and electrical properties. *Small* **16**, 1901901 (2020).
- Wu, X.-C., Tao, Y.-R. & Gao, Q.-X. Fabrication of TaS₂ nanobelt arrays and their enhanced field-emission. *Chem. Commun.* **40**, 6008–6010 (2009).
- Yoshida, M. et al. Controlling charge-density-wave states in nano-thick crystals of 1T-TaS₂. *Sci. Rep.* **4**, 7302 (2014).
- Hu, Y. et al. Toward exploring the structure of monolayer to few-layer TaS₂ by efficient ultrasound-free exfoliation. *Nanoscale Res. Lett.* **13**, 20–27 (2018).
- Nguyen, T. P. et al. Transition metal disulfide nanosheets synthesized by facile sonication method for the hydrogen evolution reaction. *J. Phys. Chem. C* **120**, 3929–3935 (2016).
- Sutto, T. E. & Averill, B. A. In *Lower-Dimensional Systems and Molecular Electronics* (eds Robert M. Metzger, Peter Day, & George C. Papavassiliou) 289–291 (Springer US, 1990).
- Zhou, L. et al. Tantalum disulfide quantum dots: preparation, structure, and properties. *Nanoscale Res. Lett.* **15**, 20 (2020).
- Kovalska, E. et al. Non-aqueous solution-processed phosphorene by controlled low-potential electrochemical exfoliation and thin film preparation. *Nanoscale* **12**, 2638–2647 (2020).
- Kovalska, E., Antonatos, N., Luxa, J. & Sofer, Z. “Top-down” arsenene production by low-potential electrochemical exfoliation. *Inorg. Chem.* **59**, 11259–11265 (2020).
- Kovalska, E. et al. Single-step synthesis of platinoid-decorated phosphorene: perspectives for catalysis, gas sensing, and energy storage. *ACS Appl. Mater. Interfaces* **12**, 50516–50526 (2020).
- Yin, H.-J., Zhou, J.-H. & Zhang, Y.-W. Shaping well-defined noble-metal-based nanostructures for fabricating high-performance electrocatalysts: advances and perspectives. *Inorg. Chem. Front.* **6**, 2582–2618 (2019).
- Konanki, S. S. & Beyette, F. R. In *2000 Digest of the LEOS Summer Topical Meetings. Electronic-Enhanced Optics. Optical Sensing in Semiconductor Manufacturing. Electro-Optics in Space. Broadband Optical Networks (Cat. No. 00TH8497)*. Publisher: IEEE, 113–114.
- Sung, S. H., Schnitzer, N., Brown, L., Park, J. & Hovden, R. Stacking, strain, and twist in 2D materials quantified by 3D electron diffraction. *Phys. Rev. Mater.* **3**, 064003 (2019).
- Li, Y., Xiao, H., Zhou, P. & Cao, J. Electronic structures of twist-stacked 1T-TaS₂ bilayers. *Phys. Lett. A* **383**, 2302–2308 (2019).
- Li, H. et al. Twisted 1T TaS₂ bilayers by lithiation exfoliation. *Nanoscale* **12**, 18031–18038 (2020).
- Wang, K. et al. Electrical control of charged carriers and excitons in atomically thin materials. *Nat. Nanotechnol.* **13**, 128–132 (2018).
- Hirata, T. & Ohuchi, F. S. Temperature dependence of the Raman spectra of 1T-TaS₂. *Solid State Commun.* **117**, 361 (2001).
- Wu, D. et al. Ultrabroadband photosensitivity from visible to terahertz at room temperature. *Sci. Adv.* **4**, eaao3057 (2018).
- Luxa, J. et al. 2H→1T phase engineering of layered tantalum disulfides in electrocatalysis: oxygen reduction reaction. *Chem. Eur. J.* **23**, 8082–8091 (2017).
- Yuan, Y.-P., Ruan, L.-W., Barber, J., Joachim Loo, S. C. & Xue, C. Heterostructured suspended photocatalysts for solar-to-fuel conversion. *Energy Environ. Sci.* **7**, 3934–3951 (2014).
- Paul, K. K. et al. Strongly enhanced visible light photoelectrocatalytic hydrogen evolution reaction in an n-doped MoS₂/TiO₂(B) heterojunction by selective decoration of platinum nanoparticles at the MoS₂ edge sites. *J. Mater. Chem. A* **6**, 22681–22696 (2018).
- Lu, Y. et al. Hierarchical CdS/m-TiO₂/G ternary photocatalyst for highly active visible light-induced hydrogen production from water splitting with high stability. *Nano Energy* **47**, 8–17 (2018).
- Najafi, L. et al. TaS₂, TaSe₂, and their heterogeneous films as catalysts for the hydrogen evolution reaction. *ACS Catal.* **10**, 3313–3325 (2020).
- Li, H. et al. Atomic-sized pores enhanced electrocatalysis of TaS₂ nanosheets for hydrogen evolution. *Adv. Mater.* **28**, 8945–8949 (2016).
- Shi, J. et al. Two-dimensional metallic tantalum disulfide as a hydrogen evolution catalyst. *Nat. Commun.* **8**, 958 (2017).
- Tong, T. et al. Sensitive and ultrabroadband phototransistor based on two-dimensional Bi₂O₃Se nanosheets. *Adv. Funct. Mater.* **29**, 1905806 (2019).
- Wen, J. et al. Ultra-broadband self-powered reduced graphene oxide photo-detectors with annealing temperature-dependent responsivity. *Carbon* **153**, 274–284 (2019).
- Long, M. et al. Room temperature high-detectivity mid-infrared photodetectors based on black arsenic phosphorus. *Sci. Adv.* **3**, e1700589 (2017).
- Bera, K. P. et al. Graphene sandwich stable perovskite quantum-dot light-emissive ultrasensitive and ultrafast broadband vertical phototransistors. *ACS Nano* **13**, 12540–12552 (2019).

ACKNOWLEDGEMENTS

We acknowledge the financial support provided by the Czech Science Foundation (GACR No. 20-16124 J). B.W. was supported from the grant of Specific university research – grant No A2_FCHT_2021_055. P.K.R. was supported by the European Structural and Investment Funds, and CHEMFELLS III' (No. CZ.02.2.69/0.0/0.0/19_074/0014006).

AUTHOR CONTRIBUTIONS

Z.S. and E.K. designed the experiment, and E.K. performed electrochemical exfoliation, microscopy and spectroscopy characterizations, photoelectrochemical

measurement, wrote the paper. P.K.R. helped with photoelectrochemical measurement and its interpretation. N.A. helped with AFM and XRD measurements. B.W. assisted with UV-VIS analysis. V.M. completed XPS and UV-VIS characterizations. M.V. performed the statistical evaluation. All the authors contributed to the writing, revision, and discussion of the manuscript.

COMPETING INTERESTS

The authors declare no competing interests.

ADDITIONAL INFORMATION

Supplementary information The online version contains supplementary material available at <https://doi.org/10.1038/s41699-021-00247-8>.

Correspondence and requests for materials should be addressed to E.K. or Z.S.

Reprints and permission information is available at <http://www.nature.com/reprints>

Publisher's note Springer Nature remains neutral with regard to jurisdictional claims in published maps and institutional affiliations.



Open Access This article is licensed under a Creative Commons Attribution 4.0 International License, which permits use, sharing, adaptation, distribution and reproduction in any medium or format, as long as you give appropriate credit to the original author(s) and the source, provide a link to the Creative Commons license, and indicate if changes were made. The images or other third party material in this article are included in the article's Creative Commons license, unless indicated otherwise in a credit line to the material. If material is not included in the article's Creative Commons license and your intended use is not permitted by statutory regulation or exceeds the permitted use, you will need to obtain permission directly from the copyright holder. To view a copy of this license, visit <http://creativecommons.org/licenses/by/4.0/>.

© The Author(s) 2021